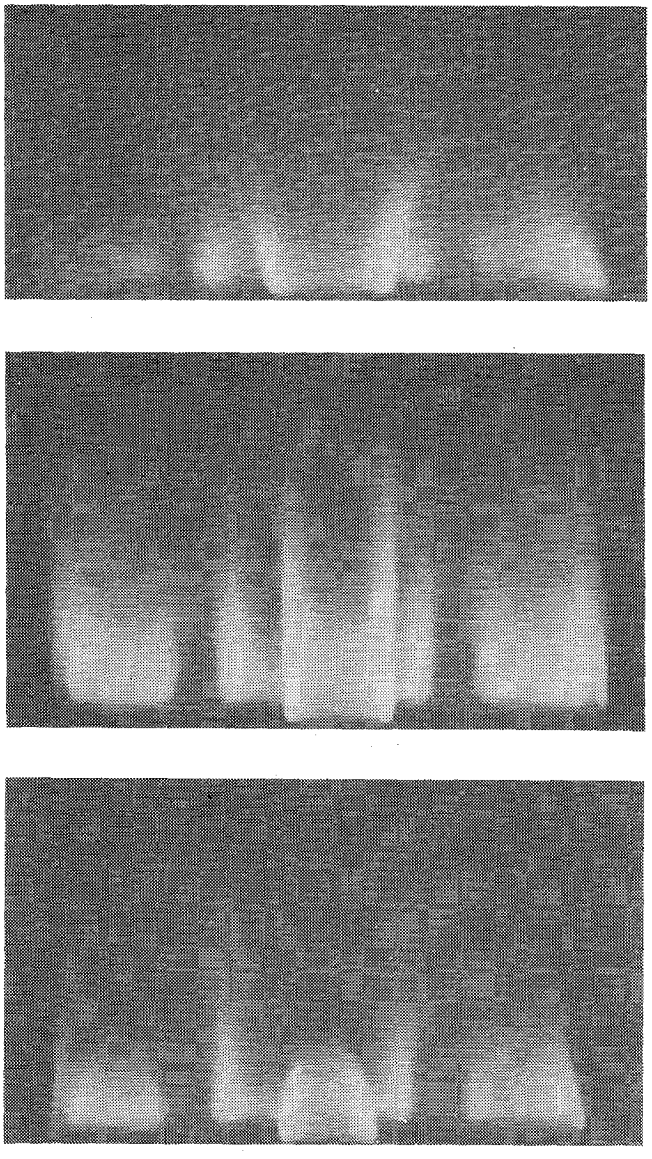

Fig. 3 Porous plate burner flames—coarse bimodal, ethane-air: a) oxidizer rich (divergent flame); b) stoichiometric (columnar flame); c) fuel rich (parabolic flame).

Flame limits encountered by independently varying fuel and oxidizer flow rates, the relative sensitivity of the fine port flames to O/F ratio, and effects of substituting oxygen for air all indicated that the fine port flames were more fuel rich. This is not surprising, since for a fixed interstitial spacing between oxidizer ports and particular values of specific flow rates, a proportionally greater amount of fuel will be associated with the fine ports. Such variable O/F ratio is a topic of current theoretical modeling of composite propellants,[4,5] but the particular allocations are not known.

Two interesting effects were noted when oxygen was substituted for air. For a given set of flow rates, the flame structure took on a less fuel-rich appearance (O/F ratio increased, as expected). Second, the porous plate became red hot in the region of the cluster of fine oxidizer ports; this confirms the higher temperature and heat feedback that would be expected with oxygen and indicates that there is more heat feedback with the fine ports. By analogy to propellants, fine particle size systems would burn faster unless the fuel allocation became such that the reduced temperature would overcome the reduced diffusion length.

Although physical overlap or intermingling between adjacent flames did not occur, two types of interaction between flames of adjacent ports were observed. First, where a fine port is adjacent to a coarse port, the fine port flame is nested under the near-surface region of the coarse port flame such that there could be heat feedback from the coarse flame to the fine flame. Second, where adjacent fine ports are sufficiently close together, the adjacent parabolic flames are joined at their bottoms by a nearly planar flame over the interstitial fuel. This feature provides a more vivid mechanism for direct heating of binder in propellants and is not predicted by current diffusion flame theory.

Conclusions

Fundamental diffusion flame data were obtained as a function of simulated oxidizer size distribution and mixture ratios utilizing a porous plate analog burner. There was much evidence in the diffusion flame structures to show that fine oxidizer ports tend to operate more fuel rich than coarse ports in a bimodal arrangement. Also, as expected, fine ports exhibited more heat feedback to the burner surface. Some interaction between flames of adjacent ports was observed, of a type that should be addressed in any future, more rigorous analytical treatment of multicomponent composite propellants.

Acknowledgments

The research described in this paper was carried out at the Jet Propulsion Laboratory, California Institute of Technology, and was sponsored in part by the Air Force Office of Scientific Research, AFOSR Support Agreement Nos. AFOSR-ISSA-79-0016 and AFOSR-ISSA-80-0017, through an agreement with NASA.

References

[1] Kumar, R. N., Strand, L. D., and McNamara, R. P., "Composite Propellant Combustion Modeling with a Porous Plate Burner," AIAA Paper 76-669, July 1976.

[2] Ramohalli, K. and Magiawala, K., "Perforated Porous Plate Burner to Model Composite Propellant Combustion," *AIAA Journal*, Vol. 19, Jan. 1981, pp. 92-93.

[3] Burke, S. P. and Schumann, T. E. W., "Diffusion Flames," *Proceedings of the First and Second Symposia on Combustion*, The Combustion Institute, Pittsburgh, Pa., 1965, pp. 2-11.

[4] Beckstead, M. W., "A Model for Solid Propellant Combustion, *Eighteenth Symposium (International) on Combustion*, The Combustion Institute, Pittsburgh, Pa., 1981, pp. 175-185.

[5] Cohen, N. S. and Strand, L. D., "A Model for the Combustion of AP Composite Propellants," AIAA Paper 81-1553, July 1981.

AIAA 80-1480R

Performance Investigation of Superfluid Heat Pipes

M. Murakami*
University of Tsukuba, Sakura, Ibaraki, Japan

Introduction

In recent years cooling to liquid helium temperature has been required for various applications. Considerable effort has been made to apply superfluid helium to cooling systems. Several space programs, such as space infrared telescopes,

Presented as Paper 80-1480 at the AIAA 15th Thermophysics Conference, Snowmass, Colo., July 14-16, 1980; submitted Jan. 20, 1981; revision received July 15, 1981.

*Lecturer, Institute of Structural Engineering. Member AIAA.

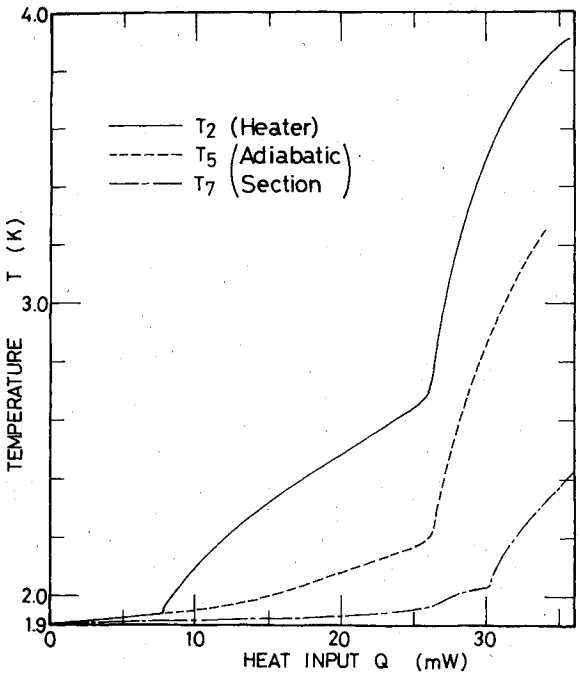

Fig. 1 Performance of superfluid heat pipe (pipe 3) as a function of heat input for sink temperature $T_s = 1.90$ K.

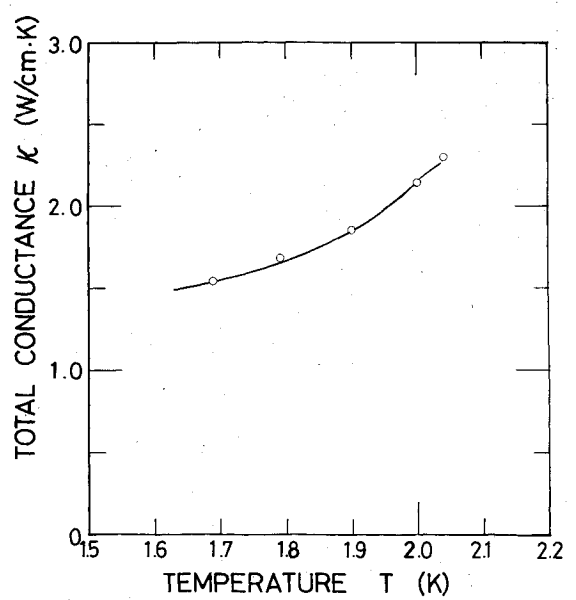

Fig. 2 Total thermal conductance vs sink temperature.

have been demanding the applications.[1] The superfluid heat pipe has been developed for such potential applications. Three superfluid heat pipes have been fabricated and tested in the course of this study. The general thermal performance of them is reported in this paper. A detailed description can be found in Ref. 2.

Heat Pipe and Test Apparatus

Superfluid phenomena can occur in adsorbed film of helium when the temperature is lowered to the lambda point ($T_\lambda = 2.172$ K). The thermomechanical effect in such films is applied to the liquid recirculation in the heat pipe. This effect makes the superfluid component in films flow toward higher temperature regions, while the normal cannot move because of its own viscosity. Thus, the working fluid is supplied to the evaporator entirely in the form of film flow. The resulting pumping capability is so large that liquid supply can be achieved overcoming vertical height as high as 1 m against the gravity. The thermal relation both at the evaporator and at the condenser is expressed by

$$Q = \dot{m}(\lambda + TS) \tag{1}$$

where Q and $\dot{m}$ are the heat input and the mass flux of the superfluid component in film, λ the latent heat of vaporization, T the temperature, and S the specific entropy. The second term of the right-hand side of Eq. (1) reflects the fact that the superfluid component flows with zero entropy.

This Note primarily is concerned with the improved model (heat pipe 3) among the three. This consists of a copper pipe with 80 fine axial grooves. A very thin perforated copper film (165 × 197 mm) folded radially is inserted in the pipe (see Ref. 2 for more details). The structure composed of a grooved pipe and a copper film is designed to increase the wetted perimeter D_w for film flow and to reduce the Kapitza thermal boundary resistance. Dimensions of the pipe are as follows: length $L = 177$ mm, o.d. = 16 mm, i.d. = 14.5 mm, total wetted perimeter $D_w = 480$ mm. The ratio of D_w to the inner circumference of a pipe with the same i.d. is about 10.5. Other heat pipes are made of a simple copper pipe with 10-mm i.d. (heat pipe 1), and of the same pipe as heat pipe 3 with smaller copper film ($D_w = 286$ mm) (heat pipe 2). All three are charged with helium gas to about 0.6 MPa under the room temperature condition, which forms enough thick superfluid film when $T < T_\lambda$.

Each one is installed vertically with the evaporator top inside a vacuum adiabatic jacket except for the condenser which is exposed to the outer HeII as a heat sink at a constant temperature. The lengths of the evaporator and the condenser are 25 and 27 mm, respectively. The pipe has an electric heater winding, and five germanium resistance thermometers, one of which monitors the sink temperature T_s.

Results and Discussions

A typical example of the steady performance is given in Fig. 1. During the test, the heater power is increased continuously at a slow rate from 0 W to about 60 mW spending about one hour as to fulfill a quasisteady heating condition. Then, it is decreased down to 0 W at the same rate. The temperature in the evaporator, T_2, rises proportionally to the heat input for small Q. At about 8 mW ($= Q_c$) a temperature jump is recorded. This results from the superfluid breakdown in the thin film. Thus, the heating condition for $Q > Q_c$ is referred to as supercritical. The temperature rise becomes large under the supercritical heating condition. The second temperature jump occurs at $Q = 26$ mW ($= Q_\lambda$). This indicates that the phase of adsorbed helium changes from superfluid to normal helium (HeII to HeI; λ-transition). Only heat conduction through the pipe wall participates in heat transfer beyond Q_λ. The temperature variations while Q is decreasing are basically coincident with those for the increasing case, but weak hysteresis are observed at $Q = Q_\lambda$ and Q_c. Temperatures in the adiabatic section are also presented by T_5 and T_7 in this figure.

The effective thermal conductance is calculated from $(T_2 - T_5)/Q$, where the cross-sectional area of the vapor core area (1.65 cm^2) is used as the heat transfer area. It is almost independent of Q and is the largest under the subcritical heating condition. It diminishes to a value given by pure thermal conduction through pipe wall beyond Q_λ. The conductance under the subcritical heating condition is plotted against the sink temperature in Fig. 2. The thermal conductivity of the pipe material (phosphorus deoxidized copper) is 0.09 W/cmK at these temperatures. It is important to note that the conductivity obtained experimentally is a total quantity which includes the effects of the Kapitza thermal resistance both at the evaporator and at the condenser. The Kapitza resistance generally exists at the interface between liquid helium and solids participating in heat transfer. The net

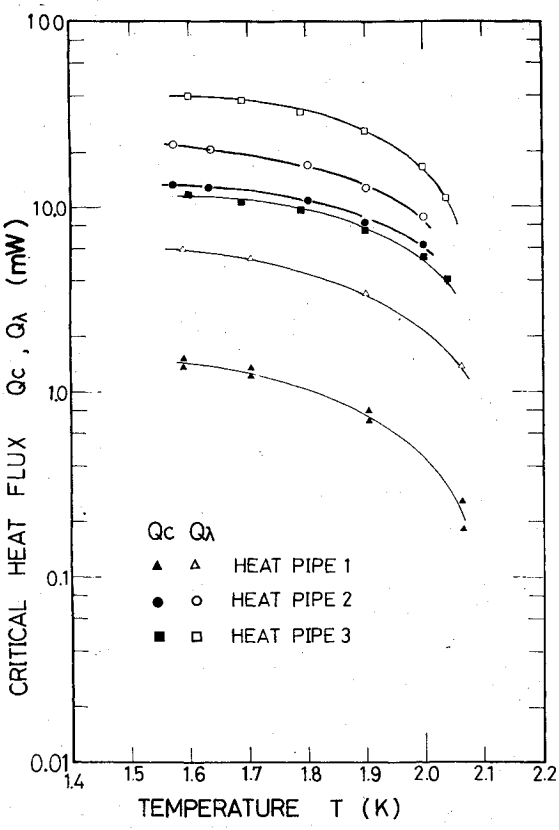

Fig. 3 Critical heat input Q_c and maximum heat transport capability Q_λ for three superfluid heat pipes.

conductance resulting only from pure heat pipe action should be much larger than the figures. In this respect, the grooved pipe is not as effective in reducing the Kapitza resistance. It is obvious that the temperature dependent property of the total conductance derives from that of the Kapitza resistance.

The heat-transport capability is evaluated by two values, Q_c and Q_λ, which are plotted vs the sink temperature in Fig. 3. The maximum heat-transport capability of the superfluid heat pipe is given by Q_λ which indicates the occurrence of the λ-transition. It is evident from this figure that Q_λ increases with D_w. This behavior suggests that the maximum heat transport capability can be improved by the increase of D_w. It has already been mentioned that the temperature jump observed at Q_c resulted from the superfluid breakdown. It characterizes an onset of energy dissipation in HeII, and does not necessarily mean that all super phenomena disappear. The superfluid heat pipe still works under supercritical heating conditions provided that $Q<Q_\lambda$. There seems to be two possible mechanisms to cause the breakdown. The first is that the breakdown occurs when local velocity of the super component of the return flow v_s exceeds its critical value v_c. The velocity reaches its maximum at the entrance to the evaporator because the film thickness decreases with the height due to the gravity effects. The breakdown first occurs there. With the increase of Q, the lower end of the active evaporating zone (evaporator + a part of the adiabatic section participating in evaporation) should go down for thicker film thickness, and the zone expands. The flow is able to be supercritical in the zone.

The breakdown phenomena can be quantitatively described in terms of the critical flow rate σ_c defined by

$$\sigma_c = v_c \delta \tag{2}$$

where δ is the film thickness. This quantity obtained experimentally was reported for various kinds of solid surfaces, on which the thin film was formed. The critical mass flow rate

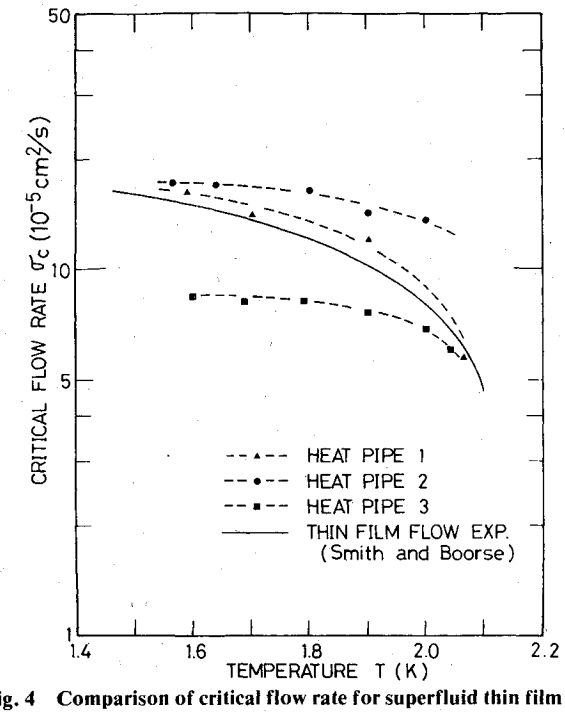

Fig. 4 Comparison of critical flow rate for superfluid thin film flow.

$\dot{m}_c$ is expressed in terms of σ_c, the super component density ρ_s and D_w by

$$\dot{m}_c = \rho_s \sigma_c D_w \tag{3}$$

Combining Eqs. (1) and (3), σ_c becomes

$$\sigma_c = Q_c / [\rho_s D_w (\lambda + TS)] \tag{4}$$

This expression suggests that Q_c is proportional to D_w and supports the idea of using a thin copper film insert in the pipe. The experimental results are given in Fig. 4 for three superfluid heat pipes together with results obtained from experiments of gravity flow of adsorbed thin film on copper surfaces.[3] It may be stated that the data from pipe 1 and 2 experiments and the thin film flow experiment are fairly close, considering that the values of Q_c differ by almost one order of magnitude and that σ_c depends on the material and the surface state on which adsorbed films are formed. This agreement indicates that the breakdown model describes fairly well the phenomena as far as pipe 1 and 2 experiments are concerned. The deviation of the pipe 3 data from the others indicates the limit of the applicability of this model. It is in the second model that the breakdown occurs when the heat flux per unit heating area q exceeds its critical value q_c. This critical value is independent of the wetted perimeter. Pipe 3 seems to be this case. The values of Q_c for pipe 3 are almost the same as those for pipe 2, although D_w of pipe 3 is almost twice as large as that of pipe 2. It can be concluded that the critical heat flux Q_c is proportional to the wetted perimeter for the film flow for small and intermediate values of the ratio of D_w to the heated perimeter, and it becomes almost independent of D_w for the larger values of the ratio.

Conclusion

This study of the superfluid heat pipe has indicated the following.

1) There are three working modes based on the magnitude of the heat load, which are clearly distinguished by large temperature jumps and hysteresis. The performance is, of course, best under the subcritical heating condition.

2) Maximum heat-transport capability can be determined by Q_λ corresponding to HeII λ-transition.

3) The critical heat load Q_c at which value the superfluid breakdown occurs increases proportionally to the wetted perimeter for the film flow for moderate values of D_w.

Acknowledgment

The axially grooved copper pipes are offered by the Furukawa Electric Co., Ltd., Tokyo.

References

[1] Vorreiter, J. W., "Cryogenics for Spacecraft," *Proceedings of 7th International Cryogenic Engineering Conference,* ICEC7, 1978, pp. 1-17.

[2] Murakami, M. and Kaido, N., "Study of Superfluid Heat Pipe," AIAA Paper 80-1480, July 1980.

[3] Smith, B. and Boorse, H. A., "Helium II Film Transport. III. The Role of Film Height," *Physical Review,* Vol. 99, July 1955, pp. 358-366.

AIAA 82-4101

Prediction of Recession Rates for Pyrolytic Graphite

H. F. Nelson*
University of Missouri-Rolla, Rolla, Mo.
and
J. N. Holsen† and A. E. Bruns‡
McDonnell Douglas Astronautics Company, St. Louis, Mo.

Introduction

A THIN coating of pyrolytic graphite can protect the structure of advanced performance ramjet combustors from oxidation by hot combustion gases for two reasons. First, the dense, nonporous pyrolytic graphite offers fewer sites for attack by oxygen than does ordinary, more porous graphite. Second, by the nature of the deposition process of pyrolytic graphite, it is primarily the relatively nonreactive basal plane that is exposed to attack. However, pyrolytic graphite is subject to oxidation, and recession rates must be used in calculating the proper coating thickness. Excess thickness increases the time and cost of the coating process and results in vehicle performance penalties.

Ramjets typically operate at temperatures near 2000 K and at pressures from 1 to 10 atm. Their exhaust contains 5-15% oxygen. For these conditions, the oxidation of pyrolytic graphite is reaction rate controlled; oxygen diffuses to the surface more rapidly than it can react at the surface. Previous studies of graphite ablation have primarily considered only molecular oxygen. However, it has been observed that at high temperatures atomic oxygen reacts with pyrolytic graphite 50-80 times as fast as molecular oxygen.[1-4]

The surface reaction rate, which is kinetically controlled, proceeds by[5]

$$C + O_2 \rightarrow CO + O \qquad (1)$$

and

$$C + O \rightarrow CO \qquad (2)$$

Reactions forming CO_2 are neglected because they are much slower. We have also neglected reactions involving gas phase molecules other than oxygen. Although H_2O and CO_2 may actively contribute to graphite oxidation, Schaefer et al.[6] present an equation for the oxidation rate of pyrolytic graphite in the presence of H_2O and CO_2 from which we estimate that the combined mass loss from those two gases is less than 1% of the expected loss from oxygen alone.

This Note compares the recession rates of pyrolytic graphite due to molecular and atomic oxygen over a wide range of ramjet operating conditions. It is concluded that the neglect of atomic oxygen can contribute errors as large as 100% in predicted pyrolytic graphite recession rates.

Molecular Oxygen Recession Rate

Nagel and Strickland-Constable[7] reported rate constants for the oxidation of pyrolytic graphite. They fit their experimental data to a surface reaction mechanism proposed by Blyholder et al.,[8] which involved two different rate equations. At temperatures below 1000 K the oxidation is described by a rate equation with an activation energy of 25 to 30 kcal/gmole. Between 1500 and 2300 K, the rate of oxidation reaches a maximum, then decreases. At still higher temperatures it increases again, following a rate equation with an activation energy between 70 and 90 kcal/gmole.

Blyholder et al. assumed two types of surface active sites to be present on carbon. The more reactive (type A) sites support the oxidation reaction at low temperatures. At higher temperatures, some type A sites are converted to less reactive (type B) sites. This accounts for the temporary decrease in the oxidation rate in the intermediate (1500-2300 K) range of temperatures. The mechanism is described by a set of three elementary reactions

	Reaction	Rate (gram atoms C/cm^2-s)	
(i)	$A + O_2 \rightarrow A + 2CO$	$r_{(i)} = k_A P_{O_2}(x)/(1 + k_z P_{O_2})$	(3)
(ii)	$B + O_2 \rightarrow A + 2CO$	$r_{(ii)} = k_B P_{O_2}(1-x)$	(4)
(iii)	$A \rightarrow B$	$r_{(iii)} = k_T(x)$	(5)

where (x) is the fraction of surface covered with type A sites; $(1-x)$ the fraction of surface covered with type B sites; P_{O_2} the partial pressure of oxygen in atmospheres, and k_A, k_B, k_z, and k_T are reaction rate constants. Applying the stationary state assumption to Eqs. (4) and (5) yields the value of x as

$$x = \left(1 + \frac{k_T}{k_B P_{O_2}}\right)^{-1} \qquad (6)$$

The recession rate in cm/s becomes

$$\dot{S}_{O_2} = \left[\frac{k_A P_{O_2}}{1 + k_z P_{O_2}}(x) + k_B P_{O_2}(1-x)\right] 12/\rho_{pg} \qquad (7)$$

using Eqs. (3) and (4), where Eq. (6) defines x. The density of pyrolytic graphite, ρ_{pg}, is assumed to be 2.20 g/cm^3 throughout this study.

Using a best fit to the experimental data, Nagle and Strickland-Constable[7] obtained the following rate constants: $k_A = 20 \exp(-30{,}000/RT_w)$; $k_B = 4.46 \times 10^{-3} \exp(-15{,}200/RT_w)$; $k_T = 1.51 \times 10^5 \exp(-97{,}000/RT_w)$; $k_z = 21.3 \exp(+4100/RT_w)$; where $R = 1.987$ cal/gmole-K and T_w is the surface temperature in K.

The recession rate is shown in Fig. 1 as a function of the wall temperature for several values of molecular oxygen partial pressure.

Received Feb. 27, 1981; revision received Aug. 14, 1981.

*Professor, Thermal Radiative Transfer Group, Department of Mechanical and Aerospace Engineering. Member AIAA.

†Technical Specialist, Technology-Thermodynamics Department. Member AIAA.

‡Lead Engineer, Technology-Thermodynamics Department. Member AIAA.